RESPONSE SIMULATION OF UHPFRC MEMBERS

Renaud Franssen[1,2], Serhan Guner[3], Luc Courard[2] and Boyan Mihaylov[2]

[1]FRIA (F.R.S.-F.N.R.S), National Fund for Scientific Research, Brussels, Belgium

[2]ArGEnCo Department, Research Unit in Urban and Environmental Engineering, University of Liège, Allée de la Découverte 9, Liège (4000), Belgium

[3]Department of Civil and Environmental Engineering, University of Toledo, 2801 W. Bancroft St., MS 307, NI 3021, Toledo, Ohio 43606-3390, USA

Abstract: Ultra-high-performance fiber-reinforced concrete (UHPFRC) is a new generation material with outstanding mechanical properties and excellent durability. The uses of UHPFRC have, however, been mostly limited to demonstration applications and research projects, due to its perceived high cost and the lack of proven analysis procedures. In the past decade, new design provisions have been proposed in France, Switzerland, Japan, and Australia while a proven numerical modeling approach is still missing. As an effort to contribute to bridging this gap, a numerical modeling approach is established in this research for UHPFRC members. The approach is based on the Diverse Embedment Model within the global framework of the Disturbed Stress Field Model, a smeared rotating-crack formulation for 2D modeling of concrete structures. This study aims to capture the behavior of UHPFRC by using only a few input parameters. The established model is validated with large-scale tests of UHPFRC beams from the literature. The beams considered incorporate various cross-section and reinforcement details, and exhibit a range of failure modes including flexure and shear. The validation studies, based on comparisons with the experimental results, demonstrate that the proposed modeling approach provides accurate response simulations through simple models with short analysis times.
Keywords: Design, finite element, nonlinear analysis, modeling, simulation, UHPFRC.

i. Introduction

The ultra-high-performance fiber-reinforced concrete (UHPFRC) has emerged in the past few decades as a new type of concrete. Based on a very fine granulometry and high ratio of cement, UHPFRC can exhibit an outstanding performance in terms of strength and durability. As compared to regular concrete, it is about five times stronger in compression with maximum strengths up to 250 MPa. The improvement is even more significant in the tensile behaviour. UHPFRC can reach 8 to 12 MPa in tension with a ductile behaviour. The durability is a consequence of the fine components used in the mixture, which creates a strong and dense matrix that is almost impermeable to water and aggressive agents from the environment. UHPFRC also permits using smaller section sizes, resulting in lighter structures and potentially more economical foundations. These properties make UHPFRC a strong candidate for the next generation infrastructure. However, despite recent code provisions from France, Switzerland, Japan, and Australia, the use of UHPFRC is still very limited. One reason for this is the lack of accurate analysis models. Most existing models are difficult to use and require many input parameters, which creates challenges for practitioners.

This study aims to establish a nonlinear finite element modeling approach to obtain accurate response simulations while using only a few input parameters. For this purpose, the Diverse Embedment Model (DEM) (Lee, Cho & Vecchio 2011), which predicts the average tensile response of FRC subjected to tension forces, is employed within the global framework of the Disturbed Stress Field Model (DSFM) (Vecchio 2000). The DSFM represents the behavior of cracked concrete based on equilibrium, compatibility of deformations and constitutive models. The established model takes account of the shear

participation of fibers and the stress-strain behavior of UHPFRC. The model is validated with fifteen rectangular and I beams from four research groups (Hussein & Amleh 2015, Randl, Mészöli & Harsányi 2018, Telleen & al. 2010, Yoo & Yoon 2015). The predicted and observed behaviors are compared in terms of stiffness, strength, post-peak response, crack pattern, and the failure mode.

ii. Proposed Modeling Approach

The finite element simulations are based on the Disturbed Stress Field Model (DSFM) for reinforced concrete proposed by Vecchio (2000). This model falls into the category of smeared rotating-crack approaches, where the crack directions coincide with the principal stress directions in the concrete, while the principal strain directions deviate due to slip displacements in the cracks. The DSFM is already implemented in the nonlinear finite element software VecTor2 (Wong, Trommels & Vecchio 2013) in a plane-stress formulation. The additional contribution of fibers in fiber-reinforced concrete is modeled with the Diverse Embedment Model (DEM) (Lee 2011) integrated in the DSFM. In this study, practical recommendations are provided on how to apply these formulation when modeling UHPFRC.

Nonlinear analysis program VecTor2 accounts for various important concrete behaviors, such as tension stiffening and compression softening. The analysis of UHPFRC requires a specific combination of material models. Table 1 summarize the suitable material models for UHPFRC as compared to the default ones for modeling RC. The results presented in this paper are all obtained with these material models.

Table 1 : Material models

Material behavior	Default models for RC	Employed models for UHPFRC
Compression pre-peak	Hognestad (parabola)	Lee et al 2011 (FRC)
Compression post-peak	Modified Park-Kent	Lee et al 2011 (FRC)
Tension softening	Bilinear	Exponential
FRC tension	SDEM - Monotonic	DEM (Lee et al 2011)
Crack width check	Agg/2.5 max crack width	5 mm max crack width

The selected models are all previously developed for the modeling of fiber reinforced concrete (FRC). The crack width check reduces the compressive strength of elements if the specified crack width is exceeded. As such, it is often used to better represent the behavior of shear-critical members with low stirrups ratios. Since aggregates sizes are very small in UHPFRC, a 5-mm max crack width option has been chosen.

The DEM is used for modeling the tension behavior of fiber-reinforced concrete. The fundamental assumption of the model is that the tensile stresses in the cracks of FRC can be expressed as the sum of the concrete and fiber contributions, adapted from Voo and Foster (2003) who developed a variable engagement model (VEM) for FRC.

While the modelling of the concrete in tension has been established in various codes and recommendations, the DEM defines the participation of the fibers as follows:

$$f_f = \alpha_f V_f \sigma_{f,cr,avg} \tag{1}$$

where f_f is the tensile stress acting on the concrete area and attributed to the fibers, α_f is a factor that accounts for fiber orientation, V_f is the fiber volumetric ratio, and $\sigma_{f,cr,avg}$ is the average fiber stress at the crack. This last quantity is obtained by double integration across all fiber angles θ and embedment lengths l_a:

$$\sigma_{f,cr,avg} = \frac{2}{l_f} \int_0^{l_f/2} \int_0^{\pi/2} \sigma_{f,cr}(l_a, \theta) \sin\theta \, d\theta \, dl_a \tag{2}$$

The modeling for UHPFRC is similar to that of RC, with some exceptions. The material models for FRC are created based on the cylinder compressive strength; all other parameters are calculated using simple equations. For high-performance fiber-reinforced materials, the modulus of elasticity is specified, which was determined from tests or was assumed to be equal to 50 GPa when test data was not available. The DSFM accounts explicitly for slip displacements in cracks. In FRC, this slip is associated with aggregate interlock shear stresses across the cracks, and the tangential stressed associated with the fibers. In the modeling of UHPFRC, the aggregate interlock is limited due to the small aggregate size (0.5-6 mm). If unknown, a conservative value of 1 mm is used in the models. Details about the modeling of the fiber stresses are provided in Lee, Cho & Vecchio (2016).

The tensile resistance due to the fibers is a function of the fiber diameter, fiber length, steel tensile strength, and the maximum bond strength between the concrete and the fibers. In both the DEM and VEM for straight fibers and regular concrete, the bond strength is defined as $\tau_{f,max} = 0{,}396\sqrt{f_c'}$ [MPa], where f_c' is the compressive strength of the concrete. For the UHPFRC, this study proposes to increase the bond resistance in recognition of the high density and high cement content of the UHPFRC matrix. Based on comparisons with tests, the value of $\tau_{f,max}$ is modified to

$$\tau_{f,max} = 0{,}75\sqrt{f_c'} \tag{3}$$

In the DSFM formulation, the predictions of the DEM are used to evaluate the stresses in the fiber-reinforced concrete in the principal tension direction. However, as the DSFM is a smeared-crack approach while the DEM focusses on a discrete crack, it is necessary to establish an accurate crack spacing measurement to link discrete values to smeared properties. Based on the studies of UHPFRC, Jungwirth and Muttoni (2008) and Sigrist and Rauch (2004) have proposed simple expression which is adopted in this study:

$$s_{cr} = 0.75\, l_f \tag{4}$$

Where l_f is the length of the fibers. The models used in VecTor2 requires a relatively limited number of input properties. Given the uniaxial compressive strength f'$_c$, an UHPFRC material can be fully described and analyzed. The geometrical properties of the fibers are also needed. Table 2 summarizes the input properties required for a sample UHPFRC material with the following properties: concrete compressive strength = 150 MPa, volume of fibers = 3%, length of the fibers = 13mm, diameter of the fibers = 0.15 mm and tensile strength of the fibers is 2500 MPa.

Table 2. Material properties

Material properties	**Value**
Initial tangent elastic mod.	50000 MPa
Max. aggregate size	1 mm
Max. crack spacing (s_{cr})	0.75*13 = 9.75 mm
All other properties	default

Smeared reinf. properties	**Value**
Fiber type	Straight
Fiber volume fraction	3%
Fiber length	13 mm
Fiber diameter	0.15 mm
Fiber tensile strength	2500 MPa
Fiber bond strength (τ_f)	$0.75x150^{0.5}$ = 9.2 MPa

iii. Validation with experiments

a. Flexure-critical beams

Flexural failure involves yielding of the longitudinal reinforcement accompanied with a local crushing of concrete in the compression zone of the section. It is a ductile failure that generally takes place with significant displacement or deflection.

The first series examined was tested by Yoo & Yoon (2015). Three beams have been modeled (NFH, S13H and S19.5 – numbers denote fiber lengths), which differ only by the length of the steel fibers. NFH is a reference test which included no fibers in the ultra-high performance concrete material. These specimens had rectangular cross sections with width of 150 mm and a depth of 220 mm. Fig 1 describes the geometrical properties of the beams while all properties can be found in Table 3. Steel plates were used at support and loading locations. The distance between load points and supports led to a shear-span-to-depth ratio equal to 5.1. The beams were loaded monotonically until failure.

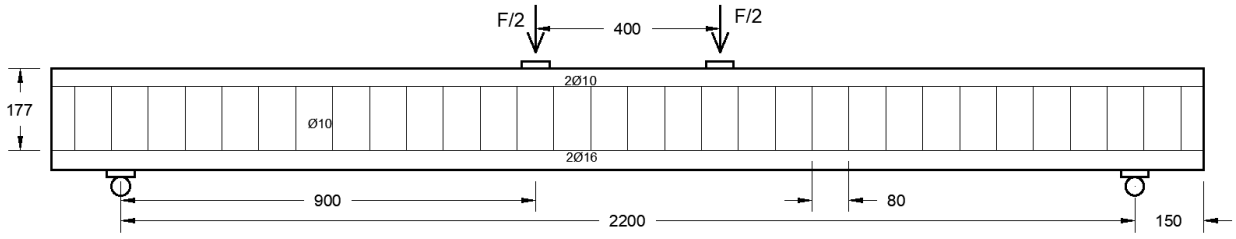

Fig 1. Test set up used by Yoo and Yoon

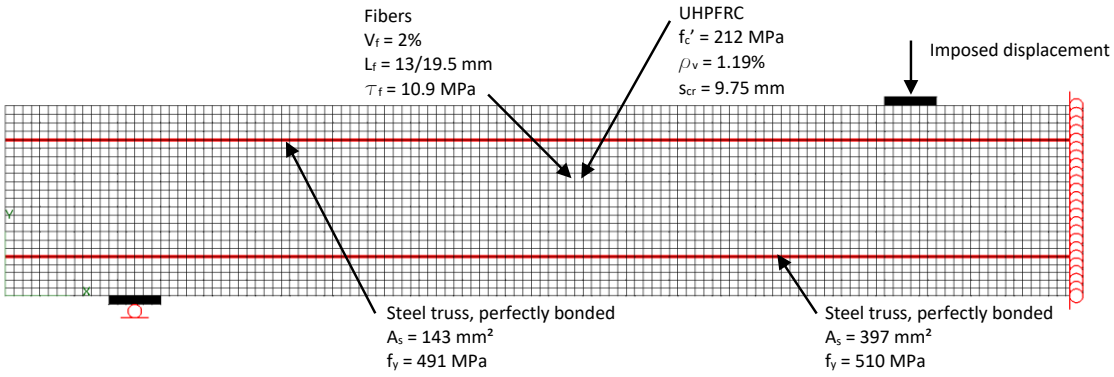

Fig 2. FEM of beams S13H and S19.5H

The finite element model of beams S13H and S19.5H is displayed in Fig 2. Quadrilateral elements are used to model UHPFRC or UHPC while discrete truss elements are used for the longitudinal reinforcement. The fibers and the stirrups are defined as smeared reinforcement. The loading is defined as displacement-controlled until the failure. The steel plates used at support and load locations are modeled as structural steel quadrilateral elements. Due to the symmetry of the test setup, the finite element model is created as one half of the specimens, and roller support are placed on the axis symmetry. A perfect bond is assumed between truss and quadrilateral elements. While Yoo & Yoon (2015) describes the complete characterization of the UHPFRC with flexural and compressive tests, only a few material properties are used to model the beams, as represented in Table 2.

Fig 3 shows the experimental and predicted load-deflection curves. All beams failed in flexure. As clear from the curves, beam NF has the largest ductility. The strength is increased from 100 kN for beam NF to 125 kN for beams with steel fibers. The flexural capacity was increased because of the strain-hardening material used. The UHPFRC was able to sustain higher loads after cracking and yielding of longitudinal bars. The use of longer fibers led to higher ductility as clear from Fig 3. Yet, the influence of fiber lengths on the stiffness of the element is found to be negligible.

The finite element model predictions are represented with the dashed lines. It can be seen that the strength predictions are satisfactory. The FEM simulations somewhat overestimated the stiffnesses. The ductility underestimation is related to the fixed crack spacing used (i.e., 9.75 and 14.63 mm for S13H and

S19.5H, respectively). These values are higher than the ones observed in the experiments. At the failure state, the sudden load drop is caused by the localization of strains and thus rapid increases in stresses in the longitudinal reinforcement.

Table 3. Tests specimens used in the validation study

	Author	Name	b (mm)	h (mm)	d (mm)	a/d	f_c' (MPa)	V_f (%)	l_f (mm)	ρ_v (%)	ρ_l (%)	P_{exp} (kN)	P_{pred} (kN)	P_{pred}/P_{exp}	Mode of failure	Cross section
1	Telleen	w	20	200	180	2.8	150	3	13	0.94	3.95	230	231	1.00	shear	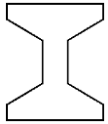
2		wo	20	200	180	2.8	150	3	13	0	3.95	184	202	1.10		
3	Randl	B15	58	350	320	3.5	166.25	2	15	1.35	3.55	479	483	1.01		
4		B17	58	350	320	3.5	170.4	2	15	0.9	3.55	446	421	0.94		
5		B19	58	350	320	3.5	174.4	2	15	0	3.55	309	319	1.03		
6		B28	58	350	320	3.5	165.8	1	15	0.9	3.55	398	394	0.99		
7		B20	58	350	320	3.5	174.4	1	15	0	3.55	258	274	1.06		
8		B18	58	350	320	3.5	174.9	0	0	0.9	3.55	253	226.2			
9	Hussein	US1-1-35	150	300	255	3.5	153	1	13	0	6.3	660	686	1.04	flexure	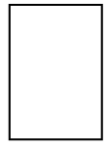
10		US1-2-35	150	300	255	3.5	159	2	13	0	6.3	724	728	1.01		
11		US1-2-2	150	300	255	2.0	155.5	2	13	0	6.3	750	773	1.03		
12		US1-2-15	150	300	255	2.0	152	2	13	0	6.3	850	932	1.10		
13	Yoo	NFH	150	200	177	5.1	202	0	0	1.19	1.5	97.9	97.5			
14		S13H	150	220	177	5.1	212	2	13	1.19	1.5	124.1	115	0.93		
15		S13L	150	220	179	5.0	212	2	13	1.19	0.94	87.3	89	1.02		
16		195H	150	220	177	5.1	210	2	19.5	1.19	1.5	125.2	134	1.07		
17		195L	150	220	179	5.0	210	2	19.5	1.19	0.94	93.3	108	1.16		
													Average	**1.03**		
													COV (%)	**5.73**		

b = minimum width of section; h= depth of section; d=effective depth of section; a= span/height of the beam subjected to constant shear; f_c'= compressive strength of UHPFRC; V_f= fiber volume ratio of the UHPFRC; l_f= fiber length; ρ_v= stirrup ratio calculated with regards to width b, ρ_l= longitudinal ratio calculated with regards to maximum width of section.

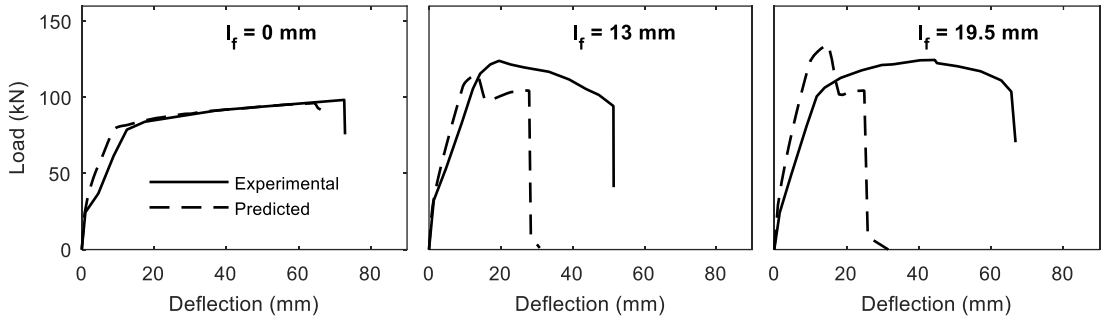

Fig 3. Measured and predicted response of beams with variable fiber length

The NLFEA is able to produce valuable insight into global structural behavior, including crack patterns and deformed shapes. Fig 4 shows the failure conditions of beams NFH and S13H. A thick red line represents crack widths larger than 2 mm. Without the presence fibers, multiple flexural thick cracks form and open. The fibers tend to bridge cracks and produce a large fan of thin cracks as presented on the right. Once the stress level reaches a certain level, the strains concentrate and one large, main crack is formed.

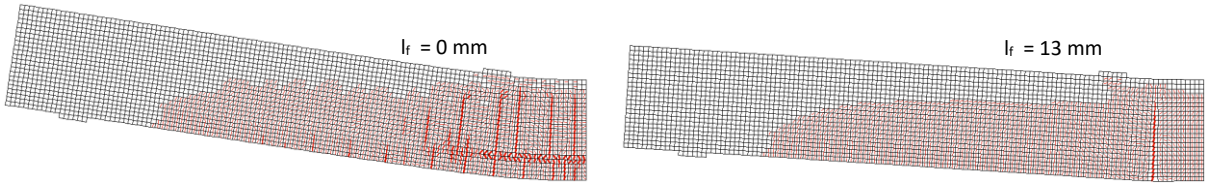

Fig 4. Crack pattern predictions at failure (post-processor Augustus, Bentz 2000)

The second sets of beams is chosen to show the influence of shear-span-to-depth (a/d) ratios. Tested by Hussein & Amleh (2014), the beams are denoted as US1-2-3.5, US1-2-2 and US1-2-1.5. They are deep beams with a/d ratios varying from 1.5 to 3.5. These beams did not contain stirrups in their effective spans. Therefore, all shear forces are carried by the direct compression strut, steel fibers (i.e., 2% in volume) and dowel action. Other important properties are listed in Table 3. The only variable between the specimens is the a/d ratio.

Beams US1-2-3.5, US1-2-2 and US1-2-1.5 failed in flexure with some ductility (see Fig 5). From the experimental results, it is clear that the longer the span, the smaller the load bearing capacity. The stiffness of the beams increases when the span decreases. The efficiency of steel fibers to sustain large shear forces is also clearly demonstrated.

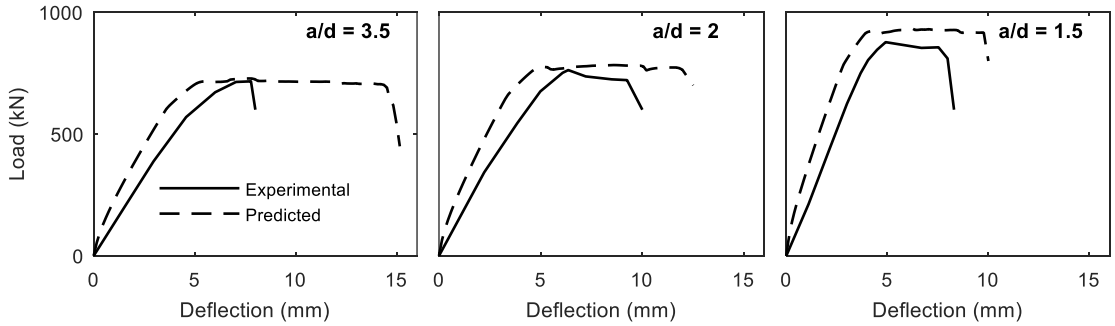

Fig 5. Measured and predicted response of beams with variable shear-span-to-depth ratio

The modeling of these beams was done similarly to the previous ones. As evident from Fig 5, the maximum load bearing capacity is well captured. The load-deflection curves are adequately predicted albeit with the ductility being slightly overestimated. The prediction of the flexural failure mode reveals that the model is able to represent the shear participation of fibers in the resistance of a structural member. These specimens would have failed in shear without the presence of fibers (Hussein, 2014).

One of the many outputs of the model process is the shear strain γ_{xy}. It represents the distortion of the elements compared to the original shape. Fig 6 displays the total shear strain for a displacement equal to 3.6 mm. The left shear span is the critical one. The right figure, representing the lower shear span ratio, shows higher shear deformations concentrated along a diagonal as opposed to the shear strains localized close to the reinforcement trusses in the left figure.

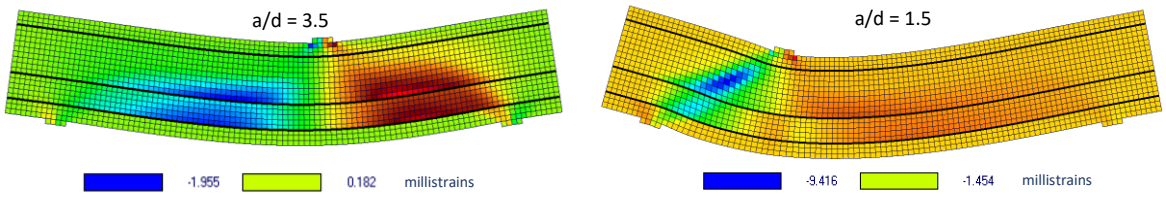

Fig 6. Predicted shear deformation at displacement equal to 3.6 mm

b. Shear-critical beams

A shear failure is typically accompanied with limited displacements, and therefore it is brittle. It usually takes place before yielding of the longitudinal reinforcement. The objective of this section is to evaluate the accuracy of the proposed modeling approach with respect to the shear resistance prediction.
The first beam set examined was tested by Randl, Mészöli & Harsányi (2018). The beams B17, B28 and B18 with I-shaped sections are shown in Fig 7. They are highly-reinforced with $7\phi 20$ at the tensile side of the section. Table 3 lists the properties of the specimens.

The modeling procedure adopted for this chapter follows the previous one used for flexure-critical beams. I-shaped sections are represented by layers of different thickness (t) to simulate the inclined parts between the web and the flanges (see Fig 7, left).

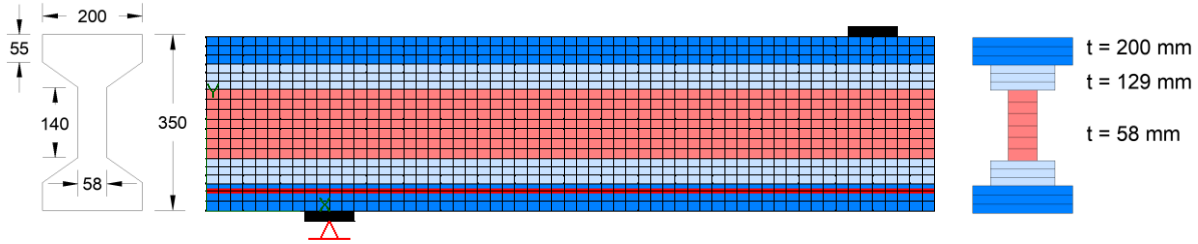

Fig 7. Cross-section and modeling approach of I beams from Randl, Mészöli & Harsányi 2018

Fig 8 presents the comparison of FE prediction and experimental load deflection curves. For beam B28, only the experimental strength is known. The experimental results shows that the load bearing capacity increases with increasing fiber ratio. Peak load ratios are 1.57 and 1.76 for B28/B18 and B17/B18, respectively. The stiffness of the specimens increases as the ratio of fibers increases. The FEM captured the influence of fibers on the maximum deflections. The load bearing capacities are also well predicted.

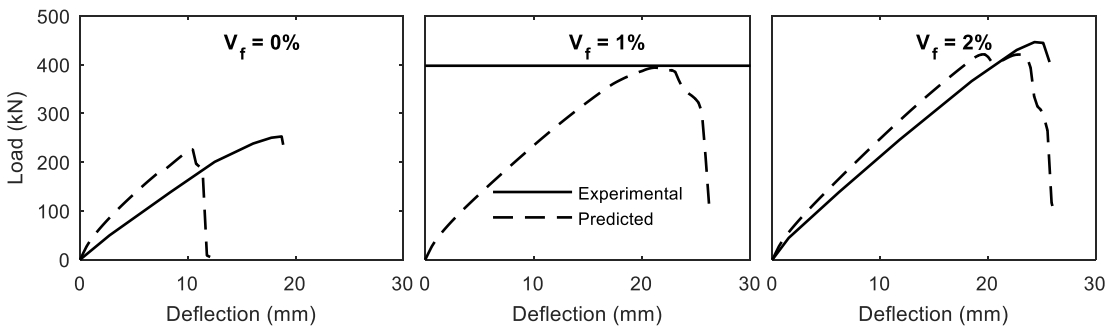

Fig 8. Measured and predicted response of beams with variable steel fiber ratio

The last set of tests examined here was designed to study the influence of stirrups in the shear resistance of I beams. Tested by Telleen & al. (2010), the material properties of these beams are listed in Table 3. The comparison between experimental and predicted results is presented in Fig 9. During the experiments, it was observed that the resilience of beams with stirrups was higher than those without stirrups. This behavior and the load bearing capacity is reasonably well represented by the FE model. As expected, the member with stirrups reached a higher capacity.

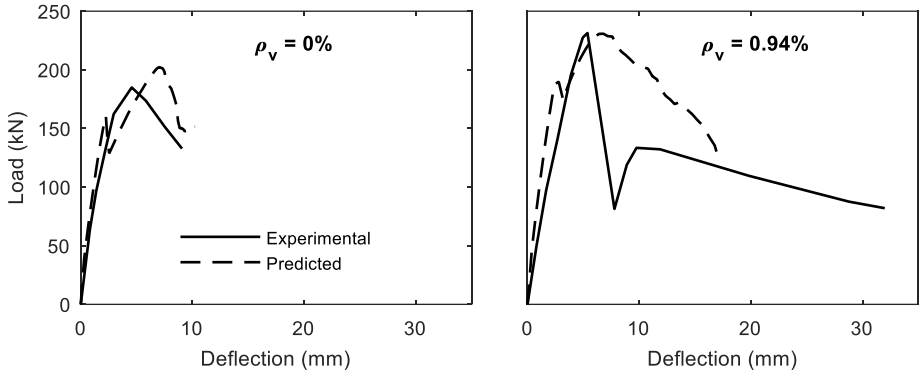

Fig 9. Measured and predicted response of beams with variable stirrups ratio

Fig 10 presents the crack patterns at the failure of the beam without stirrups. The measured and predicted crack patterns are similar with a main diagonal crack in the web causing the failure. This crack is inclined at about 45° from the point load and propagates horizontally along the web to the supports. A large set of small cracks develops with the same inclination in both spans. This was captured by the model where crack spacing is fixed to 13x0.75 = 9.75 mm and one element has a size of 10x10 mm.

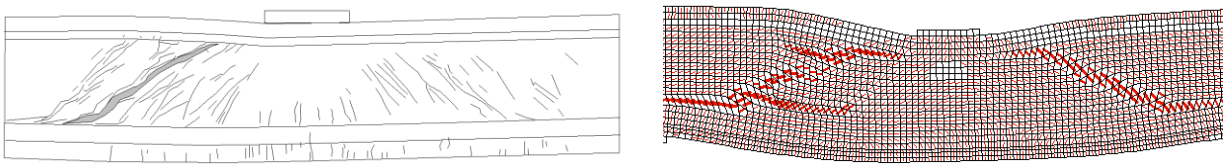

Fig 10. Measured and predicted (post-processor Augustus (Bentz 2000)) crack patterns at failure of beam without stirrups from Telleen (2010)

Fig 11 summarizes the strength predictions of all fiber-reinforced beams modeled in this study. The x-axis represent the shear-span-to-depth ratio or the volume of fibers while the y-axis represents the ratio between the finite element model predictions and the experimental results. This figure shows the accuracy of the proposed modeling approach, with ratios close to unity. Considering all specimens, an average ratio of 1.03 with a COV of 5.7% is obtained.

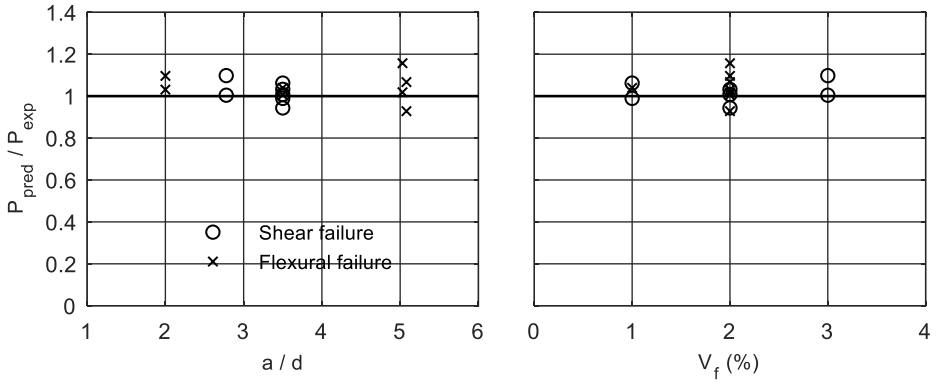

Fig 11. Experimental-to-predicted ratios for 15 UHPFRC beams

iv. Summary and conclusions

A modeling approach for modeling UHPFRC has been presented. Using currently-available formulations and software, this new approach is described with the intention that practicing engineers and researchers can follow the same modeling strategies. The approach is validated with large-scale experimental specimens available in the literature. The comparisons between the experimental and simulated results are made in terms of maximum capacity, post-peak behavior, stiffness, ductility, and cracking behavior. Based on the results obtained, the following conclusions are reached:

1. The material behavior models employed in this study provided accurate results for the analysis of UHPFRC members. For the eight flexure-critical beams, the average experimental-to-predicted beam strength ratio is 1.04 with a coefficient of variation (COV) of 6.97%. For the seven shear-critical beams the ratio is 1.02 with a COV of 4.93%.
2. The proposed modeling approach requires a few material properties, derived from a standard uniaxial compression strength f'_c.
3. The proposed modeling approach is shown to exhibit no bias with respect to the UHPFRC properties (V_f, f'_c), geometry (a/d) or steel reinforcement details (ρ_v , ρ_l). It is, therefore, found to be applicable to general modeling cases involving UHPFRC.
4. The reader can reproduce the results obtained in this study or perform new analysis using the proposed modeling approach.
5. This method requires short analysis times. The longest time required in this study was 15 min. using a laptop computer with Intel Core i5-6440HQ processor, 16 GB RAM, and 256 GB Solid State hard drive.

v. References

1. Bentz, E.C., "Sectional Analysis of Reinforced Concrete Members", Ph.D. thesis, Department of Civil Engineering, University of Toronto, 2000, Toronto, Canada.
2. Deluce, J.R., Lee, S.-C. et al., "Crack Model for Steel Fiber-Reinforced Concrete Members

   Containing Conventional Reinforcement", ACI Structural Journal, 111(1), 2014, pp 93-102, http://vectoranalysisgroup.com/journal_publications.html.
3. Hussein, L., Amleh, L., "Structural behavior of ultra-high performance fiber reinforced concrete-normal strength concrete or high strength concrete composite members", Construction and Building Materials, 93, 2015, pp 1105-1116.

4. Jungwith, J., Muttoni A., "Structural Behavior of Tension Members in UHPC", Proceedings of the International Symposium on Ultra High Performance Concrete, Kassel, Germany, 2004, pp 533-546.
5. Sigrist, V., Rauch, M., "Deformation behavior of reinforced UHPFRC elements in tension", Tailor Made Concrete Structures - Walraven & Stoelhorst (eds), 2008, pp 405-410.
6. Lee, S.-C., Cho, J.-Y. et al, "Analysis of Steel Fiber-Reinforced Concrete Elements Subjected to Shear", ACI Structural Journal, 113(2), 2016, pp 275-285, http://vectoranalysisgroup.com/journal_publications.html.
7. Lee, S.-C., Cho, J.-Y. et al., "Diverse Embedment Model for Steel Fiber-Reinforced Concrete in Tension: Model Development", ACI Structural Journal, 108(5), 2011, pp 516-525, http://vectoranalysisgroup.com/journal_publications.html.
8. Lee, S.-C., Oh, J.-H. et al, "Compressive behavior of fiber-reinforced concrete with end-hooked steel fibers", Materials, 8(4), 2015, pp 1442-1458, http://vectoranalysisgroup.com/journal_publications.html.
9. Randl, N., Mészöli, T. et al, "Shear Behaviour of UHPC Beams with Varying Degrees of Fiber and Shear Reinforcement", High Tech Concrete: Where Technology and Engineering Meet, D. Hordijk and M. Luković, eds., 2018, Springer, Cham, Switzerland.
10. Telleen, K., Noshiravani, T. et al, "Experimental investigation into the shear resistance of a reinforced UHPFRC web element", Proceedings, 8th fib PhD Symposium in Kgs. 2010, Lyngby, Denmark.
11. Vecchio, F.J., Collins, M.P., "The Modified Compression-Field Theory for Reinforced Concrete Elements Subjected to Shear", ACI Journal, 83(2), 1986, pp 219-231, http://vectoranalysisgroup.com/journal_publications.html
12. Vecchio, F.J., "Disturbed Stress Field Model for Reinforced Concrete: Formulation", Journal of Structural Engineering, 97(1), 2000, pp 102-110, http://vectoranalysisgroup.com/journal_publications.html.
13. Voo, J.Y.L., Foster, S.J., "Variable Engagement Model for Fiber-Reinforced Concrete in Tension", Uniciv Report No. R-420, School of Civil and Environmental Engineering, University of New South Wales, 2003.
14. Wong, P., Trommels, H. et al., "VecTor2 and FormWorks Manual", 2013, Toronto, Canada, http://vectoranalysisgroup.com/user_manuals.html.
15. Yoo, D.-Y., Yoon, Y.-S., "Structural performance of ultra-high-performance concrete beams with different steel fibers", Engineering Structures, 102, 2015, pp 409-423.